

# “Barber pole turbulence” in large aspect ratio Taylor-Couette flow

A. Prigent and O. Dauchot

*Service de Physique de l’Etat Condensé, CEA Saclay, 91191 Gif sur Yvette, France*  
(April 26, 2024)

Investigations of counter-rotating Taylor-Couette flow (TCF) in the narrow gap limit are conducted in a very large aspect ratio apparatus. The phase diagram is presented and compared to that obtained by Andereck *et al.* [1]. The spiral turbulence regime is studied by varying both internal and external Reynolds numbers. Spiral turbulence is shown to emerge from the fully turbulent regime via a continuous transition appearing first as a *modulated* turbulent state, which eventually relaxes locally to the laminar flow. The connection with the intermittent regimes of the plane Couette flow (pCf) is discussed.

47.20.Ft 47.20.Ky 47.54.+r, 47.27.Cn

The “barber pole structure of turbulence” [2] between two counter-rotating cylinders, also called spiral turbulence, is commonly described as alternating helical stripes of laminar and turbulent flow. There are few quantitative studies of this puzzling regime, where long range order coexists with small scale turbulence. In early studies Coles and Van Atta [3–5] measured the spiral shape in the mid-plane perpendicular to the cylinder axis and the pattern rotation rate. Later Andereck *et al.* reported qualitative observations when varying  $R_i$  [1]. Hegseth *et al.* [6,7] described spiral turbulence within the framework of phase dynamics. All these studies were limited by their relatively small size. Only one helical turbulent stripe, winding no more than twice along the cylinder axis, could be observed. Altogether, the origin of this flow pattern remains unknown.

Performing measurements in large aspect ratio Taylor-Couette flow, we show that the spiral turbulence bifurcates continuously from the turbulent flow, appearing as a modulated turbulent state. After a rapid description of the experimental set up, we present the phase diagram and compare it to the one obtained by Andereck *et al.* [1] with a different cylinder radius ratio. Then we describe the successive steps leading to the fully turbulent flow before discussing the origin of spiral turbulence. Finally, we examine its breakdown into a spatio-temporal disordered regime similar to the laminar-turbulent coexistence dynamics observed in plane Couette flow [8,9].

Let us recall here the characteristics of the experimental set up [10]. Our TC apparatus, two coaxial cylinders of radius  $r_i = 49.09 \pm 0.005$  mm and  $r_o = 49.95 \pm 0.005$  mm with a useful length  $L = 380 \pm 0.1$  mm, rotating independently, has a gap size  $d = 0.863 \pm 0.01$  mm, large aspect ratio  $\Gamma_z = L/d = 442$  and  $\Gamma_\theta = \pi(r_i + r_o)/d = 362$ , and a radius ratio  $\eta = 0.983$  very close to 1. In this paper, length and time units are  $d$  and  $d^2/\nu$ .  $\eta$  being fixed, the flow is governed by the inner and outer Reynolds numbers  $R_{i,o} = r_{i,o}\Omega_{i,o}d/\nu$ , with  $\Omega_{i,o}$  the angular velocities, and  $\nu$  the kinematic viscosity. The accuracy of  $R_{i,o}$  is better than 3%.

We visualize the flow by a “fluorescent lighting” technique [10] developed for this study. The water flow is seeded with Kalliroscope AQ 1000 ( $6 \times 30 \times 0.07 \mu\text{m}$  platelets). The inner cylinder is covered by a fluorescent film and the entire apparatus is UV-lighted. The fluorescent film re-emits a uniform visible lighting, transmitted through the fluid layer: the more turbulent the flow, the brighter it appears. As the gap is very thin, the Kalliroscope concentration is increased up to 25% by volume to enhance the contrast. A rheological study has shown that the fluid remains Newtonian, so that the only impact is a viscosity increase up to  $\nu = 1.13 \cdot 10^{-6}$  m<sup>2</sup>/s at 20°C. The flow is thermalized by water circulation inside the inner cylinder. At thermal equilibrium the temperature is uniform in space up to 0.1°C and does not vary more than 0.1°C/hour. Images and spatio-temporal diagrams (temporal recording of one line along the cylinder axis) are recorded by a CCD camera. Two plane mirrors reflect the two thirds of the flow hidden to the camera so that the whole cylindrical flow can be reconstructed.

Coles [3] has stressed the variety of flow structures observed according to the path followed in parameter space. The experimental procedure followed here is the most frequent one. The outer cylinder is slowly accelerated to the desired angular velocity while the inner one is at rest. Then, the inner cylinder is slowly accelerated ( $(1/\Omega_i) \cdot (\partial\Omega_i/\partial t) = 0.03\%$  per second) in order to ensure quasi-static transitions. (It was checked that the Taylor vortices threshold is determined with an accuracy better than 1% as soon as the acceleration rate is less than 0.05%). Recording the various flow regimes in parameter space ( $R_i, R_o$ ), gives the experimental phase diagram (fig. 1(a)) to be compared to that given by Andereck *et al.* [1] for a different geometry ( $\eta = 0.878$  and much smaller aspect ratio). The same regimes are observed but their locations in the parameter space change. The linear thresholds increase (at  $R_o = 0$ , the Taylor vortices appear for  $R_i^* = 320$  instead of  $R_i^* = 120$ ). This was expected in regards of the plane Couette flow limit and agrees very well with Snyder’s law  $R_i^* = 27[(1 - (\eta))\eta]^c - 5/3$  [11].

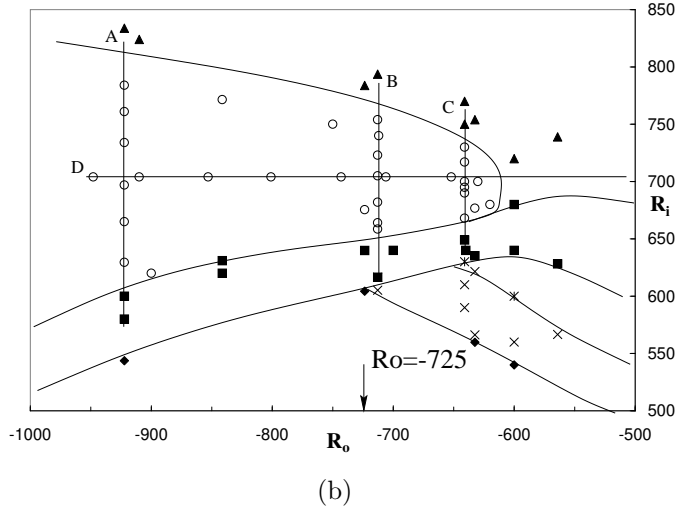
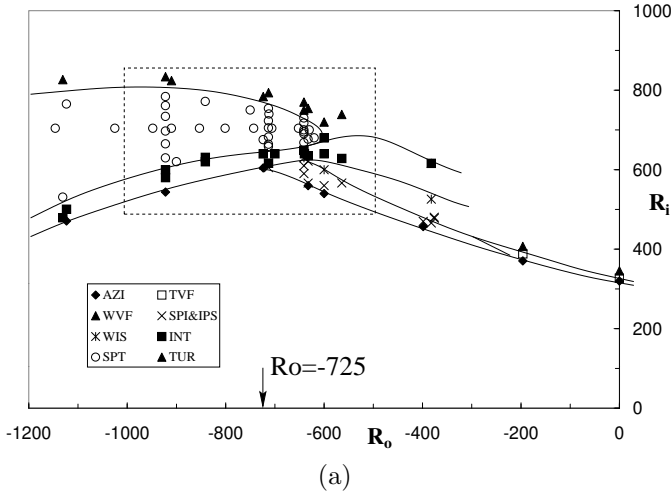


FIG. 1. Experimental phase diagram ( $\eta = 0.983$ ). (b) displays a zoom of the dotted rectangle of (a). The labels stand for AZI : azimuthal flow; TVF: Taylor vortex flow; WVF: wavy vortex flow; SPI&IPS: spiral and interpenetrating spiral vortices; WIS: wavy interpenetrating spiral vortices; INT: intermittency; SPT: spiral turbulence; TUR: turbulence. The arrow indicates the  $R_o$  value below which the AZI flow jumps directly to INT (see text for details). The solid straight lines in (b), show the paths along which measurements are conducted (A:  $R_o = -922$ ; B:  $R_o = -713$ ; C:  $R_o = -641$ ; D:  $R_i = 704$ ).

Accordingly, the other vortex flows (WVF, SPI, IPS...) also appear at higher  $R_i$  values. Second, the laminar-turbulent coexistence regions (INT and SPT), extend to higher  $R_o$  values. Finally, for  $R_o < -725$ , the azimuthal flow jumps directly to INT whereas, for  $R_o > -725$ , it bifurcates first to IPS or SPI.

Figure 2, shows snapshots of the whole flow, along paths A and C. For  $R_o = -922$ , the boundaries trigger turbulent stripes are at  $R_i$  lower than the expected linear instability threshold (fig. 2(a)). In fig. 2(b) periodically organized turbulent stripes have formed: spiral turbulence is established as a regular rotating pattern with uniform pitch angle along the cylinder axis.

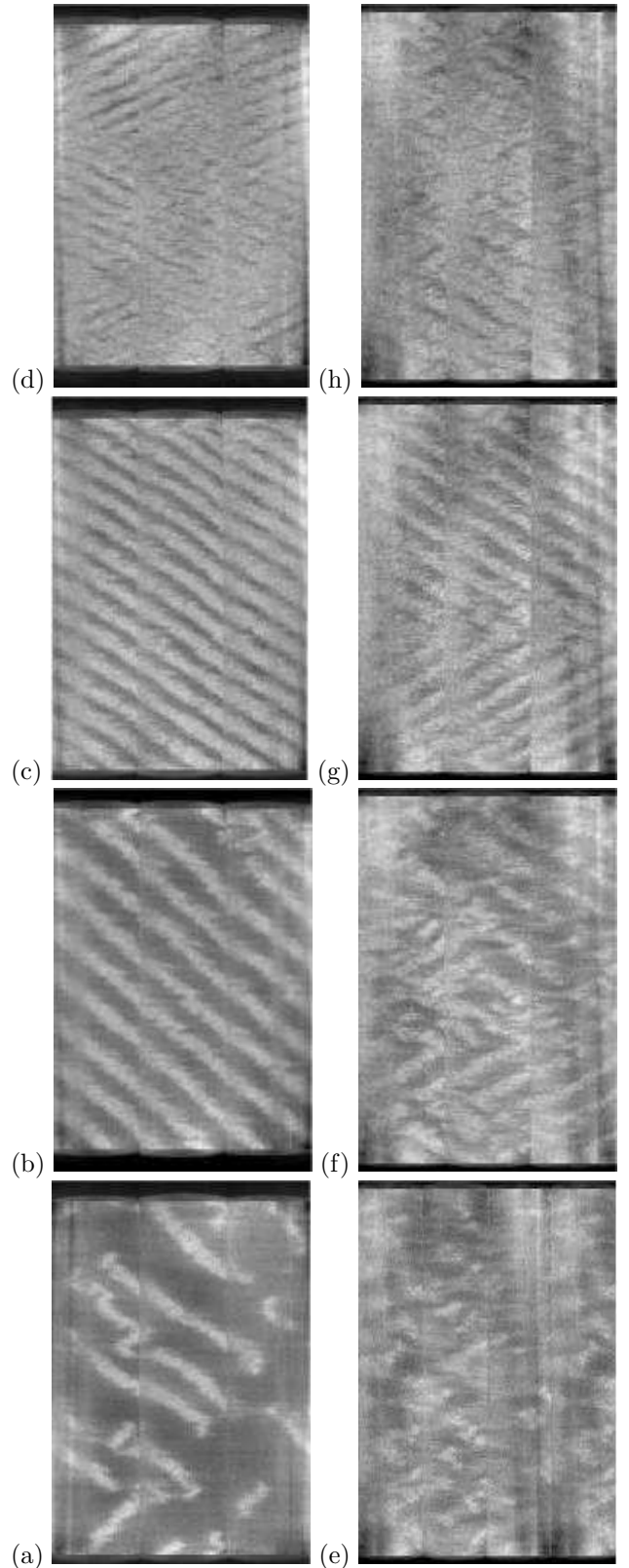


FIG. 2. Turbulent spots and stripes along paths A and C. Left column is path A,  $R_o = -922$ :  $R_i =$  (a) 580, (b) 600, (c) 697, (d) 784. Right column is path C,  $R_o = -641$ :  $R_i =$  (e) 649, (f) 668, (g) 695, (h) 717. Each picture displays a  $360^\circ$  view of the whole flow (38 cm high and 31.4 cm wide).

Further increasing  $R_i$ , the pattern maintains itself and the number of stripes increases (fig. 2(c)). Finally, the pattern disappears smoothly as homogeneous turbulence takes over (fig. 2(d)). In this regime, one notices several domains of opposite pitch spirals. For  $R_o = -641$ , the azimuthal flow first bifurcates to a vortex flow, within which, further increasing  $R_i$ , turbulent spots follow an intermittent bursting dynamics (fig. 2(e)). In fig. 2(f), the spots grow, merge and build up the turbulent spiral pattern. For illustration, we show, in fig. 2(g), two opposite pitch spirals competing and leading to a so-called “V”-shaped pattern. In figure 2(h), spiral turbulence turns into uniform turbulence as for  $R_o = -922$ . Fig. 3 displays the spatio-temporal dynamics of a front between two opposite spirals. This front, moving along the cylinder axis, is eventually absorbed at one of the extremities.

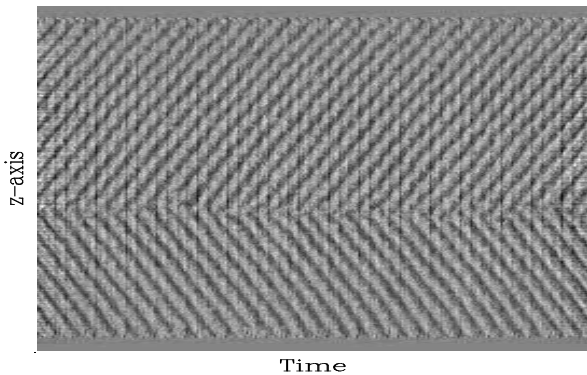


FIG. 3. Spatio-temporal diagram of spiral turbulence displaying a front between two domains of opposite pitch angle.  $R_o = -838$ ,  $R_i = 707$ . The z-axis display the whole flow height (38 cm) and the total recording length is 20.48 s.

Let us now consider the previous scenario in reverse. Decreasing  $R_i$ , spiral turbulence appears from homogeneous turbulence. At  $R_i = R_{ic}$ , a low amplitude modulation, with wave vector  $k$  and frequency  $\omega$ , uniformly emerges from the turbulent flow with no preferred direction. A slow front dynamics occurs between domains of opposite pitch until the  $z \rightarrow -z$  symmetry breaks and selects a single uniform spiral. Further decreasing  $R_i$ , the modulation amplitude increases until a more complex dynamics occurs. The light intensity, which in the first approximation corresponds to the turbulence level, is recorded in spatio-temporal diagrams such as fig. 3. In the following, we obtain the amplitude  $A$ , the axial component  $k_z$  of the wave vector and the frequency  $\omega$  of the light intensity modulation by demodulation [12]. Owing to the azimuthal periodicity, the azimuthal component of the wavevector,  $k_\theta = 2.n_\theta/(r_i + r_o)$ , is quantized,  $n_\theta$  being the number of pattern periods along one perimeter.

Four paths in the  $(R_o, R_i)$  plan are investigated. We first consider the three vertical paths A, B and C ( $R_o = -922$ ,  $R_o = -713$  and  $R_o = -641$ ).

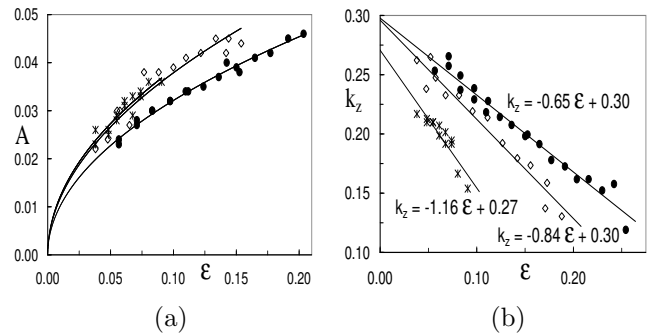


FIG. 4. The spiral turbulence amplitude (a) and vertical wave number (b) vs.  $\epsilon$ . ( $R_o = -641$  (\*),  $R_o = -713$  ( $\diamond$ ),  $R_o = -900$  ( $\bullet$ )).

Fig. 4(a) displays the amplitude of the wave against the threshold distance  $\epsilon = |R_i - R_{ic}|/R_{ic}$ .  $R_{ic}$  is determined by extrapolation, assuming a linear dependence of  $A^2$  on  $R_i$ , as suggested by the general framework of amplitude equations. The resulting values,  $R_{ic} = 820$  for  $R_o = -922$ ,  $R_{ic} = 785$  for  $R_o = -713$  and  $R_{ic} = 740$  for  $R_o = -641$ , agree with the observed thresholds. The axial component  $k_z$  of the wavevector decreases linearly with  $\epsilon$  from a critical value  $k_z^c$  close to 0.30 (see fig. 4(b)). As long as the spiral is well defined, the azimuthal wave number  $n_\theta$  equals 6 along paths A and B and 5 along path C.  $n_\theta$  being constant and  $k_z$  decreasing with  $\epsilon$ , the spiral pitch,  $\phi = \arctan(k_\theta/k_z)$ , increases with  $\epsilon$  from a critical value  $\phi^c = 18^\circ$  up to  $40^\circ$ .

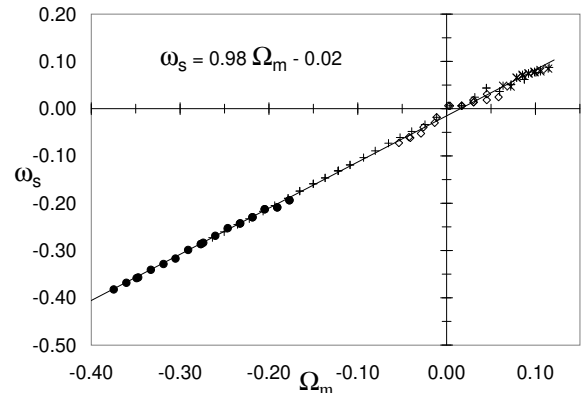


FIG. 5. The angular velocity  $\omega_s$  vs.  $\Omega_m$ , ( $R_o = -641$  (\*),  $R_o = -713$  ( $\diamond$ ),  $R_o = -900$  ( $\bullet$ ) and  $R_i = 704$  (+)).

We now consider the horizontal path D with  $R_i = 704$ . For  $R_o > -630$ , the flow is fully turbulent. Decreasing  $R_o$ , spiral turbulence emerges from the fully turbulent regime. The initial azimuthal wave number  $n_\theta = 5$  increases to  $n_\theta = 6$  by Eckhaus-like re-arrangements. The axial wave vector component remains constant on the explored values  $-950 < R_o < -630$ . Finally, fig. 5 displays  $\omega_s = \omega/n_\theta$ , the angular velocity of the spiral turbulence pattern, vs.  $\Omega_m = \frac{1}{2}(\Omega_i + \Omega_o)$ . As seen by Coles and Van Atta [3–5], the pattern rotates with the mean angular velocity of the two cylinders ( $\omega_s = \Omega_m$ ) and not with the outside cylinder as reported by Andereck *et al.* [1] as well

as by Goharadzeh and Mutabazi [13]. In the latter study, the range of variation for  $\Omega_i/\Omega_o$  is actually too small to distinguish a dependence on  $\Omega_o$  from one on  $\Omega_m$ .

Altogether, the spiral turbulence emerges as a wavy turbulent state pattern, which bifurcates continuously from the homogeneous turbulent flow. This wavy behavior agrees with the idea of a phase dynamics analysis suggested by Hegseth *et al.* [6,7] to describe the pitch variation, they observed. However the present study does not report any pitch variation. In their analysis, Hegseth *et al.*, on the basis of the mean flow measurements by Coles and Van Atta [5], suggest that the spiral turbulence induces a backflow, whose mean axial component is differently modified at both extremities. The resulting different pitches locally imposed in the boundary conditions drive the pitch variation along the axis. In the present study, both the large aspect ratio and the gap thinness considerably reduce the backflow and the influence of the end boundaries.

For low values of  $R_i$ , we observed disconnected turbulent domains surrounded by a laminar flow, which evokes the transitional dynamics observed in the plane Couette flow [14], where turbulent domains move, grow, decay, split and merge leading to the so-called spatio-temporal intermittency (STI), a process in which active/turbulent regions may invade absorbing/laminar domains out of which disorder cannot spontaneously emerged [15]. Considering the vicinity of the plane Couette flow limit,  $\eta = 1$ , and following Colovas and Andereck [16], one would like to know whether Taylor-Couette flow actually exhibits STI and how the flow evolves from a continuous turbulent state modulated in space and time to two-state coexistence. In a first attempt to answer these questions, we binarized the flow into alternating laminar and turbulent domains as is common in an STI context. This first-order approximation should not influence the results presented below, at least at a qualitative level.

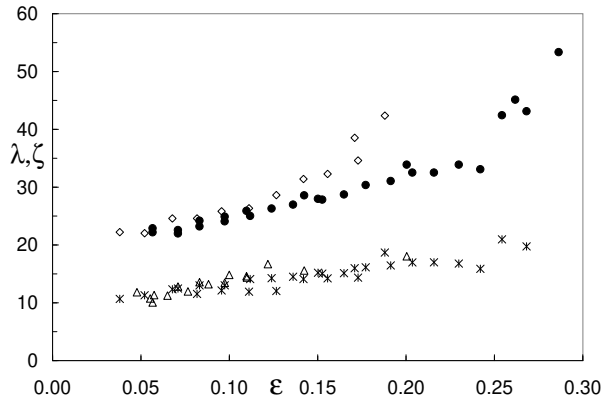


FIG. 6.  $\lambda$  ( $R_o = -713$  ( $\diamond$ ) and  $R_o = -922$  ( $\bullet$ )), the pattern wavelength and  $\zeta$  ( $R_o = -713$  ( $\triangle$ ) and  $R_o = -922$  ( $*$ )), the turbulent stripes width, against  $\epsilon$ .

Fig. 6 displays the turbulent stripes width,  $\zeta$ , and the wavelength,  $\lambda$  of the spiral pattern, parallel to the wave vector direction.  $\lambda$  increases faster than  $\zeta$ : the minima of

the modulation becomes more and more distant from the most active turbulent regions. Simultaneously the modulation amplitude increases and these minima are less and less turbulent. As a result they become areas favorable to local relaxation to the laminar flow and the modulated turbulent state turns into a periodic pattern of alternating turbulent and laminar stripes separated by fronts. This totally different spatio-temporal dynamics rapidly turns into the disordered STI regime.

Our very large aspect ratio TC apparatus has allowed, for the first time, to visualize and quantitatively analyse the “barber pole turbulence” at large scales. First, this study brings quantitative evidence of the spatio-temporal periodicity of the pattern and its dependence on control parameters. Second, it shows that the spiral turbulence, previously described as alternating turbulent and laminar bands, actually appears through a modulation of the homogeneous turbulent state. To our knowledge, it is the first time that the transition from homogeneous turbulence to spiral turbulence is investigated. Finally measurements of the turbulent stripes width relatively to the pattern wavelength have allowed us to describe the relaxation mechanism followed between the modulated turbulent state and the laminar-turbulent coexistence.

We thank H. Chaté, P. Manneville and I. Mutabazi for fruitful discussions, and C. Gasquet and V. Padilla for technical assistance.

- 
- [1] C. D. Andereck, S. S. Liu and H. L. Swinney, *J. Fluid Mech.* **164**, 155 (1986).
  - [2] R. P. Feynman, *Lecture Notes in Physics* (Addison-Wesley Reading, MA, 1964), vol. 2.
  - [3] D. Coles, *J. Fluid Mech.*, **21**, 385 (1965).
  - [4] C. Van Atta, *J. Fluid Mech.*, **25**, 495 (1966).
  - [5] D. Coles and C. W. Van Atta, *Phys. of Fluids Supp.*, S120 (1967).
  - [6] J. Hegseth, C. D. Andereck, F. Hayot and Y. Pomeau, *Phys. Rev. Letters*, **62**, 257 (1989).
  - [7] J. Hegseth, C. D. Andereck, F. Hayot and Y. Pomeau, *Eur. J. Mech. B*, **10**, 221 (1991).
  - [8] O. Dauchot and F. Daviaud, *Phys. of Fluids*, **7**, 335 (1995).
  - [9] S. Bottin and H. Chaté, *Eur. Phys. J. B*, **6**, 143 (1198).
  - [10] A. Prigent and O. Dauchot, submitted to *Physics of Fluids* (1999).
  - [11] H. A. Snyder, *The Physics of Fluids*, **11**, 1599 (1968).
  - [12] V. Croquette and H. Williams, *Physica D*, **37**, 300 (1989).
  - [13] A. Goharadzeh and I. Mutabazi, in *2<sup>ime</sup> Colloque sur le Chaos temporel et le Chaos spatio-temporel*, Rouen (1998).
  - [14] S. Bottin, F. Daviaud, P. Manneville and O. Dauchot, *Eur. Phys. Lett.*, **43**, 171 (1998).
  - [15] H. Chaté and P. Manneville, in *Turbulence, A tentative dictionary*, P. Tabeling and O. Cardoso Eds., New York, p 111-116, Plenum Press (1994).
  - [16] P. W. Colovas and C. D. Andereck, *Phys. Rev. E*, **55**, 2736 (1997).